RSC Advances

PAPER

View Article Online
View Journal | View Issue

Cite this: RSC Adv., 2016, 6, 57098

Organic sodium terephthalate@graphene hybrid anode materials for sodium-ion batteries†

Ying Wang, Katja Kretschmer, Jinqiang Zhang, Anjon Kumar Mondal, Xin Guo and Guoxiu Wang*

Received 6th May 2016
Accepted 7th June 2016

DOI: 10.1039/c6ra11809g

www.rsc.org/advances

In the search for high-performance electrodes for sodium-ion battery applications, there is a high demand for organic materials with satisfactory electrochemical performances, especially high rate capabilities. Herein, we report an organic based composite, sodium terephthalate@graphene (Na_2TP@GE) hybrid synthesized *via* freeze-drying technique. This material shows an interconnected, multi-channelled monolith structure, which resulted in outstanding rate capability for sodium storage. This hybrid material demonstrated a high reversible capacity of 268.9 mA h g^{-1} and prolonged cyclability with capacity retention of 77.3% over 500 cycles.

Introduction

As the most promising alternative candidates for the next generation battery systems, rechargeable sodium-ion (Na-ion) batteries have gained great interest over the last few years.[1–3] Conventionally, anode materials for Na-ion batteries include carbonaceous materials, metal oxides and phosphates, and alloys.[4] However, unlike commercialized carbonaceous materials in lithium-ion (Li-ion) battery systems, sodium atoms barely intercalate into graphitic carbons.[5,6] In addition, the use of metal oxides and metal alloys as electrode materials is far from renewable, not to mention the sluggish intercalation of sodium and extremely poor cyclability in the case of Si, Ge, Sb and Bi *etc.*[7–10] Therefore, intensive efforts have been made in searching for suitable organic materials that possess the advantages of electrochemical activity and natural abundance, while being environment-friendly, which make the concept of clean energy possible.

The first small-molecule based organic electrode was reported by D. L. Williams in 1969,[11] followed by extensive investigations on lithium-containing carbonyl-based organics,[12,13] carboxylate,[14–16] oxocarbons,[17,18] and polyketones.[19,20] Na-ion battery operation resembles the reaction mechanism of Li-ion batteries and the potential difference between lithium and sodium metal is only 0.3 V, suggesting the feasibility and availability of organic materials for Na-ion batteries. For instance, K. Amine's group surveyed a series of organic carboxylate based materials as the anode materials for Na-ion batteries.[21] They exhibited a long discharge plateau below 0.6 V *vs.* Na/Na^+. Jun Chen's group investigated the electrochemical performance of $Na_4C_8H_4O_4$, which can be used as both positive and negative electrode material in Na-ion batteries.[22] Furthermore, Yong Lei's group reported several conjugated organic carboxylates, which demonstrated that molecular design is an effective way to improve the electrochemical performances of organic material.[23]

Recently, sodium terephthalate $Na_2C_8H_4O_4$ (Na_2TP) is gaining extensive attention and has shown reliable electrochemical properties in terms of high sodium storage capacity, good cycling performance and rate capability. The first publication about Na_2TP demonstrated a high reversible capacity of 250 mA h g^{-1} and good cyclability,[24] resembling the crystal structure and electrochemical properties of lithium terephthalate ($Li_2C_8H_2O_6$, Li_2TP).[16] However, due to the intrinsic poor conductivity of organic materials, they usually suffer from poor rate capability for sodium storage.[20] In this paper, bare Na_2TP was synthesized from low-cost terephthalic acid, which is commonly used as a precursor for the polyester PET. To improve the electron conductivity of bare Na_2TP, graphene was used to modify bare Na_2TP *via* a freeze-drying technique, followed by heat treatment at mild temperature.[25] The physical properties and electrochemical performances of the sodium terephthalate@graphene (Na_2TP@GE) hybrid were systematically investigated.

Experimental

Materials preparation

Bare sodium terephthalate $Na_2C_8H_4O_4$ (Na_2TP) was prepared *via* a modified acid–base reaction based on the previous report.[26] Terephthalic acid was used as the starting material, which is available in abundance from the recycling of polyethylene

Centre for Clean Energy Technology, School of Mathematical and Physical Sciences, University of Technology Sydney, NSW 2007, Australia. E-mail: Guoxiu.wang@uts.edu.au

† Electronic supplementary information (ESI) available: Nuclear magnetic resonance data, thermogravimetric analysis and scanning electron microscopy. See DOI: 10.1039/c6ra11809g

terephthalate. In a typical procedure, 0.02 mol of terephthalic acid was added into 10 mL sodium hydroxide solution (0.066 mol) with deionized water gradually added up to 50 mL until the full dissolution of the Na_2TP. The aqueous solution was slowly evaporated to collect the Na_2TP crystals, which were further purified with copious ice-cold ethanol and dried at 120 °C for 12 h in vacuum.

Graphene oxide (GO) was synthesized by a modified Hummer's method.[27] Typically, natural graphite flakes (1.0 g, Sigma-Aldrich), $NaNO_3$ (1.0 g), and H_2SO_4 (98 wt%, 48 mL) were mixed and stirred in an ice bath, and $KMnO_4$ (6 g) was slowly added into the mixture. After mixing for 30 min, the ice bath was removed and the mixture was further stirred for another 48 h. Next, distilled water (90 mL) was added under stirring, while the temperature rose to 60 °C. Finally, H_2O (240 mL, 60 °C) was added, followed by the slow addition of H_2O_2 (15 mL, 30%). The final suspension was centrifuged, filtered and washed with water several times to obtain graphene oxide. The as-synthesized graphene oxide was dispersed into distilled water and sonicated for 2 h to form a homogeneous suspension of GO/H_2O.

Na_2TP@GE hybrid was synthesized *via* a freeze-drying technique. Firstly, 30 mg Na_2TP powder was added into 5 mL GO/H_2O suspension (3.0 mg mL^{-1}) to form a transparent brownish solution, which underwent freeze-drying at −80 °C for 48 h until complete dryness. Afterwards, the as-synthesized powder was ground and sintered at 300 °C for 2 h in Ar. As Na_2TP is highly soluble in water, the graphene content in the Na_2TP@GE hybrid was determined by dissolving this composite in copious water and collection of the filtrate, which was further purified and dried in an oven overnight. The final graphene content was 22 wt%.

Structural and physical characterization

The crystal structure and phase purity of the as-prepared materials were characterized by X-ray powder diffraction (XRD), nuclear magnetic resonance (NMR) and Fourier transform infrared spectroscopy (FTIR). XRD data were collected on a Siemens D5000 Diffractometer with Cu Kα radiation (λ = 0.15405 nm) in the 2θ range of $10 \leq 2\theta \leq 60°$ at a scanning step of 0.02° s^{-1}. NMR spectra were recorded on an Agilent 500 spectrometer at room temperature. Samples were dissolved in D_2O prior sealing in a 5 mm NMR tube. FTIR was carried out using a Nicolet Magna 6700 FT-IR spectrometer. All spectra were obtained using 4 cm^{-1} resolution and 64 scans at room temperature. The thermal stability of bare Na_2TP was determined by thermogravimetric analysis (TG, TA Instruments) using an SDT 2960 simultaneous DTA/TGA analyzer from RT to 800 °C at a heating rate of 5 °C min^{-1} in air. The morphologies were analyzed *via* field emission scanning electron microscopy (FESEM, Zeiss Supra 55VP).

Cell assembly and electrochemical testing

The electrochemical tests of both bare Na_2TP and Na_2TP@GEhybrid *versus* sodium were carried out in coin cells assembled inside an argon-filled glove box (Unilab, Mbraun, Germany). The bare Na_2TP electrodes were made from 55 wt% active materials, 30 wt% carbon black, and 15 wt% polyvinylidene fluoride (PVDF), while the Na_2TP@GE hybrid electrode were prepared from 85 wt% active materials and 15 wt% PVDF. For each cell, the loading mass was about 1 mg cm^{-2} and the electrolyte was a solution of 1 M $NaClO_4$ in a mixture of ethylene carbonate (EC) and propylene carbonate (EC : PC = 1 : 1 volume ratio), in which 5 vol% fluoroethylene carbonate (FEC) was added as the electrolyte additive. To exclude the capacity contribution of carbon materials to the total capacity of the electrode, background tests were carried out on bare carbon black and bare graphene, respectively. Both electrodes were made from 85 wt% carbon materials and 15 wt% PVDF. The charge–discharge tests were performed between 0.01–2.0 V on a Neware battery tester at various current densities.

Results and discussion

The synthetic process of the Na_2TP@GE hybrid architecture is shown in Scheme 1. First, the GO suspension was prepared *via* a modified Hummer's method. Second, the as-prepared Na_2TP was added into the GO suspension according to the desired ratio. Afterwards, the Na_2TP@GO suspension was frozen immediately after the full dissolution of Na_2TP salts. Finally, the Na_2TP@GE hybrid was obtained *via* the freeze-drying of the Na_2TP@GO suspension, which has been reported beneficial for electrochemical performance,[28–30] followed by mild-temperature sintering. The phases of Na_2TP and Na_2TP@GE were characterized by XRD and are shown in Fig. 1(a) and (b), respectively. The XRD patterns of both samples unveil that Na_2TP is single phase and has an orthorhombic structure, which can be indexed to the space group $P2_1/c$ with JCPDS card no. 00-052-2146.[31] As shown in Fig. 1, both XRD patterns resemble each other with the peak intensities of Na_2TP@GE hybrid much lower than that of the bare Na_2TP, indicating the much smaller

Scheme 1 Schematic illustration of the formation of Na_2TP@GE hybrid.

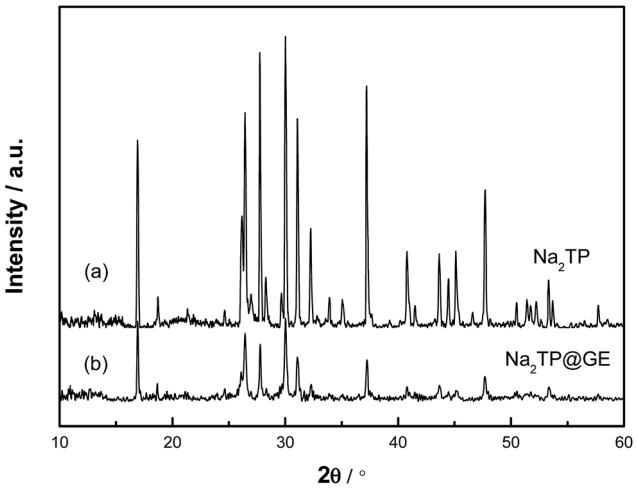

Fig. 1 XRD of (a) bare Na_2TP and (b) Na_2TP@GE composite materials.

particle size of the hybrid than the bare sample. The structure of Na_2TP is further confirmed by ^1H and ^{13}C NMR (Fig. S1†).

Fig. 2 compares the FTIR spectra of terephthalic acid, bare Na_2TP and Na_2TP@GE. The broad peak at 940 cm^{-1} corresponds to O–H bending vibrations of the carboxyl (COOH) group in the terephthalic acid raw material. After the synthetic reaction, it clearly shows the disappearance of O–H bend bond from the raw material, which has resulted from the sodium insertion into the molecule to form the disodium terephthalate. The absorption bands at 1394 and 1566 cm^{-1} are attributed to the C–C stretching vibration from the aromatic structure. Meanwhile, the FTIR spectra of bare Na_2TP and Na_2TP@GE show the same peak positions, suggesting the subsequent graphene modification process does not affect the phase of Na_2TP. In addition, Fig. S2† displays the thermogravimetric analysis of bare Na_2TP, and demonstrates its high thermal stability with less than 1 wt% weight loss up to 500 °C in air. The morphology of bare Na_2TP and Na_2TP@graphene hybrids was revealed by FESEM imaging displayed in Fig. 3. In detail, Fig. 3(a) shows that the bare Na_2TP exhibited irregular particles with a size in micrometre range. The high-magnification image in Fig. 3(b) reveals a flake-like structure of the bare Na_2TP with tens of microns in size. On the contrary, the Na_2TP@GE hybrid demonstrates a regular monolith structure with well-ordered multiple channels (Fig. 3(c)) achieved by the freeze-drying method. The zoom-in image of the white rectangular area of Fig. 3(c) is shown in Fig. 3(d) and it can be clearly seen that the ordered channels are interconnected. These channels are beneficial for the electrolyte penetration and electron transfer which will lead to much improved electrochemical properties when used as the electrode material in Na-ion battery applications. More FESEM images of the Na_2TP@GE hybrid are shown in Fig. S3†, which further confirm its unique nanoarchitecture.

The electrochemical performances of both bare Na_2TP and Na_2TP@GE were tested in a voltage range of 0.01–2 V *vs.* Na^+/Na at different current densities. Cycling performances of pristine carbon black and graphene are shown in Fig. S4† as the background tests.

All the electrochemical properties of bare Na_2TP and Na_2TP@GE hybrid were calculated based only on the weight percentage of organic material in each electrode. Discharge curves for the 2nd, 100th, 250th and 500th cycles are shown in Fig. 4(a) and (b), respectively. Both samples displayed similar charge–discharge profiles with the potentials dropping dramatically to reach a plateau of around 0.29 V, which are related to the desodiation of sodium ions from Na_2TP,[24] indicating that the presence of graphene did not affect the reaction mechanism of Na_2TP. Theoretically, the reaction mechanism of sodium terephthalate *vs.* sodium can be expressed as $Na_2C_8H_4O_4 \xleftrightarrow{2Na^+ + 2e^-} Na_4C_8H_4O_4$ with the two carbonyl groups allowing for the intercalation and deintercalation of two Na ions into its molecular structure, resulting in a specific capacity of 255 mA h g^{-1}. In the first cycles, it is noticeable that both bare Na_2TP and Na_2TP@GE produced large irreversible capacity loss.

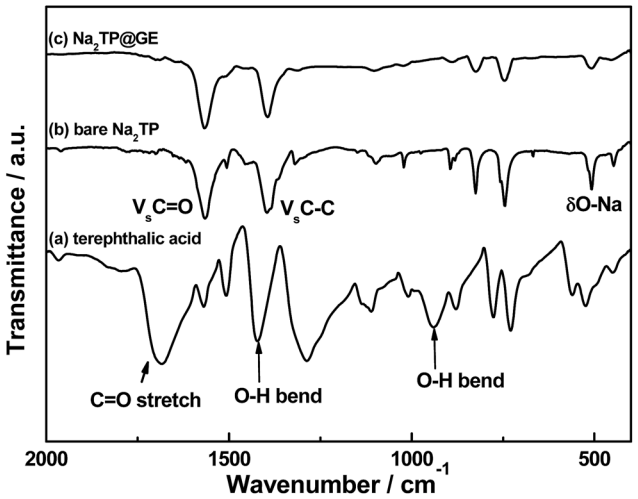

Fig. 2 FTIR spectra of (a) terephthalic acid, (b) bare Na_2TP and (c) Na_2TP@GE hybrid.

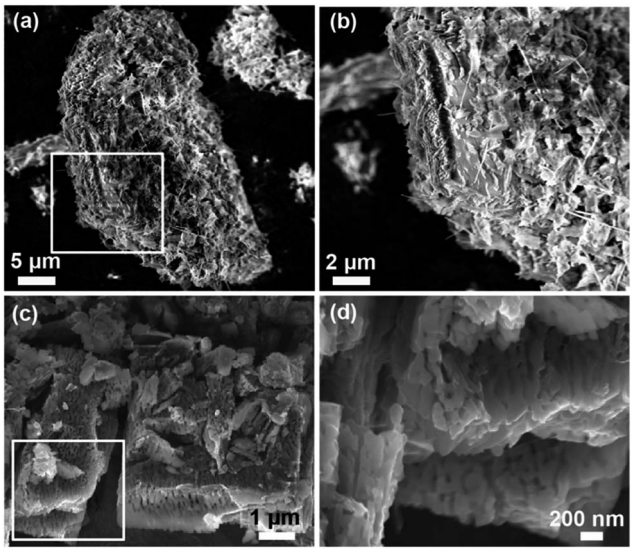

Fig. 3 FESEM images of (a), (b) bare Na_2TP and (c), (d) Na_2TP@GE hybrid at different magnifications.

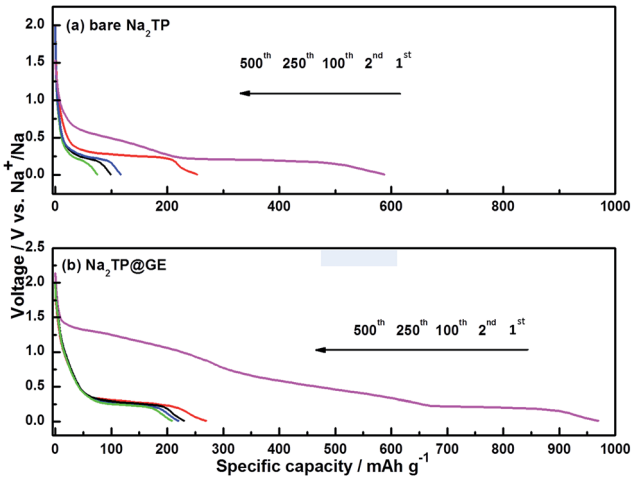

Fig. 4 Discharge profiles of (a) bare Na_2TP and (b) Na_2TP@GE hybrid at selected cycle numbers at a current density of 100 mA g^{-1}.

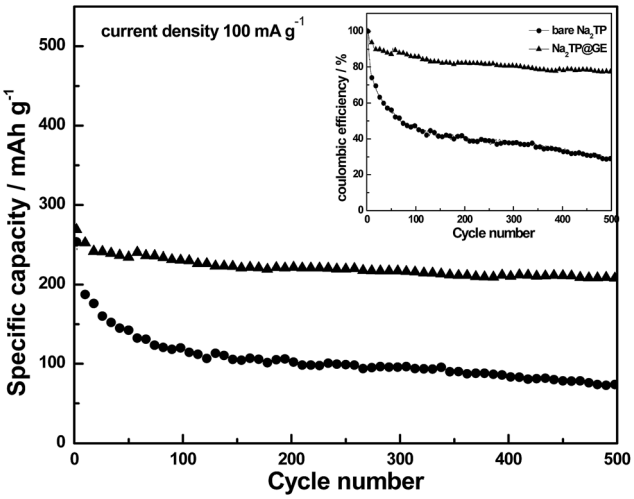

Fig. 5 Cycling performances of bare Na_2TP (circle) and Na_2TP@GE hybrid (triangle) for 500 cycles (corresponding coulombic efficiencies shown in the inset).

This is related to the irreversible decomposition of the electrolytes to form solid electrode interface (SEI) resulting relatively low coulombic efficiencies in the first cycle. At the 2nd cycle, the discharge capacities of bare Na_2TP and Na_2TP@GE are 253.5 mA h g^{-1} and 268.9 mA h g^{-1}, respectively, which are close to the theoretical capacity of Na_2TP. During the subsequent cycles, the specific capacity of bare Na_2TP decays dramatically, while the Na_2TP@GE hybrid exhibited outstanding cyclability, delivering much higher discharge capacities than those of the bare Na_2TP. To be specific, at the 250th cycle, the Na_2TP@GE hybrid electrodes delivered a discharge capacity of 219.7 mA h g^{-1}, which is much higher than the discharge capacity of bare Na_2TP (98.97 mA h g^{-1}) and previous reports.[21,24] It should be noted that during the following charge–discharge process, the discharge profiles of Na_2TP@GE composite traced back very well and showed excellent reversibility, suggesting fast electron transfer in the Na_2TP@GE materials. On the contrary, the discharge voltage plateau of bare Na_2TP was decreasing while cycling, revealing the large polarization and poor reversibility of this material.

Fig. 5 further compares the cycling performances and their corresponding coulombic efficiencies of bare Na_2TP and Na_2TP@GE hybrid. The Na_2TP@GE hybrid electrode showed to have much higher coulombic efficiency than that of the bare Na_2TP. However, both samples coulombic efficiencies are still quite low compared with the conventional Li-ion batteries. This might be related to the side reactions involved during the electrochemical process in the Na-ion battery system, which needs to be further improved. After 500 cycles, 77.3% of the Na_2TP@GE hybrid electrode's initial capacity (207.9 mA h g^{-1}) was found to be retained, compared to 29.3% (74.3 mA h g^{-1}) of the initial bare Na_2TP capacity, indicating the Na_2TP@GE hybrids are highly reversible towards sodium insertion. The rate performances of bare Na_2TP and Na_2TP@GE are evaluated based on the profile of the charge–discharge current densities shown in Fig. 6.

At a low current density of 100 mA g^{-1}, there is less difference in discharge capacity between both samples. However,

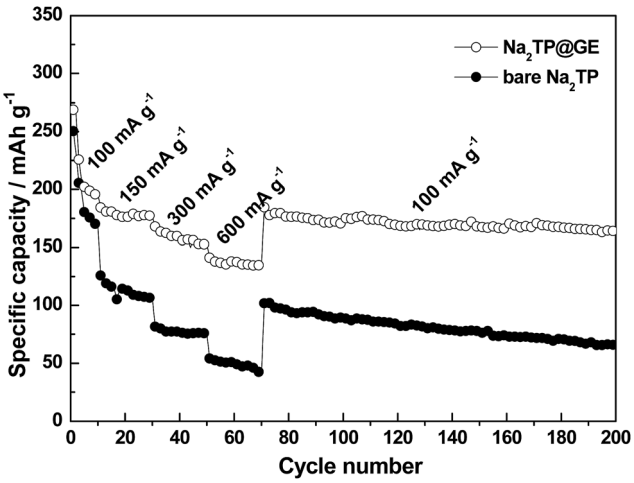

Fig. 6 Rate performances of bare Na_2TP and Na_2TP@GE hybrid at various current densities.

when the current densities are increased to 300 mA g^{-1}, the composite electrode delivered twice the discharge capacity of the bare one, with the values of 168 mA h g^{-1} and 81.5 mA h g^{-1}, respectively. Even at a high current density of 600 mA g^{-1}, the Na_2TP@GE hybrid electrodes were still able to maintain a reversible discharge capacity of 141 mA h g^{-1}, while the bare electrode only reached less than 54 mA h g^{-1}. It is worth noting that when the cells continued cycling at the original low current density of 100 mA g^{-1}, the hybrid electrodes recovered well and delivered a capacity of around 184.6 mA g^{-1}.

Conclusions

The Na_2TP@GE hybrid was prepared by a freeze-drying method. FESEM analysis confirmed that Na_2TP@GE hybrid showed a well-constructed multi-channelled structure, with well

retained graphene layers after freeze-drying. The electrochemical properties of both bare Na_2TP and Na_2TP@GE hybrid have been fully evaluated through a series of electrochemical tests. The hybrid electrode delivered a high reversible capacity of 268.9 mA h g^{-1}, and high capacity retention of 77.3% after 500 cycles. In addition, at elevated cycling current densities, the Na_2TP@GE hybrid exhibits more than twice the reversible capacities of the bare one. The improved electrochemical performances of Na_2TP@GE can be ascribed to its unique nanoarchitecture with multi-channelled monolithic grains beneficial for fast intercalation of sodium ions during the prolonged charge–discharge process. The graphene layers maintain well separated *via* freeze-drying, which leads to synergetic effects in preventing particle agglomeration, enhancing electronic conductivity of the insulating Na_2TP, while maximizing reaction sites for electrochemical reactions. The Na_2TP@GE hybrid is a promising organic hybrid material for high-performance Na-ion batteries.

Acknowledgements

This project is financially supported by the Australian Renewable Energy/Agency (ARENA) project (ARENA 2014/RND106).

References and notes

1 M. D. Slater, D. Kim, E. Lee and C. S. Johnson, *Adv. Funct. Mater.*, 2013, **23**, 947–958.
2 S.-W. Kim, D.-H. Seo, X. Ma, G. Ceder and K. Kang, *Adv. Energy Mater.*, 2012, **2**, 710–721.
3 D. Kundu, E. Talaie, V. Duffort and L. F. Nazar, *Angew. Chem., Int. Ed.*, 2015, **54**, 3431–3448.
4 X. Xiang, K. Zhang and J. Chen, *Adv. Mater.*, 2015, **27**, 5343–5364.
5 R. Alcantara, J. M. Jimenez-Mateos, P. Lavela and J. L. Tirado, *Electrochem. Commun.*, 2001, **3**, 639–642.
6 S. Wenzel, T. Hara, J. Janek and P. Adelhelm, *Energy Environ. Sci.*, 2011, **4**, 3342–3345.
7 L. Baggetto, J. K. Keum, J. F. Browning and G. M. Veith, *Electrochem. Commun.*, 2013, **34**, 41–44.
8 B. Farbod, K. Cui, W. P. Kalisvaart, M. Kupsta, B. Zahiri, A. Kohandehghan, E. M. Lotfabad, Z. Li, E. J. Luber and D. Mitlin, *ACS Nano*, 2014, **8**, 4415–4429.
9 L. Wu, H. Lu, L. Xiao, J. Qian, X. Ai, H. Yang and Y. Cao, *J. Mater. Chem. A*, 2014, **2**, 16424–16428.
10 Y. Zhao and A. Manthiram, *Chem. Mater.*, 2015, **27**, 3096–3101.
11 D. L. Williams, J. J. Byrne and J. S. Driscoll, *J. Electrochem. Soc.*, 1969, **116**, 2.
12 X. Han, C. Chang, L. Yuan, T. Sun and J. Sun, *Adv. Mater.*, 2007, **19**, 1616.
13 Z. Song, Y. Qian, M. L. Gordin, D. Tang, T. Xu, M. Otani, H. Zhan, H. Zhou and D. Wang, *Angew. Chem., Int. Ed.*, 2015, **54**, 13947–13951.
14 X. Wu, J. Ma, Y.-S. Hu, H. Li and L. Chen, *J. Energy Chem.*, 2014, **23**, 269–273.
15 L. Fedele, F. Sauvage and M. Becuwe, *J. Mater. Chem. A*, 2014, **2**, 18225–18228.
16 M. Armand, S. Grugeon, H. Vezin, S. Laruelle, P. Ribiere, P. Poizot and J. M. Tarascon, *Nat. Mater.*, 2009, **8**, 120–125.
17 H. Chen, M. Armand, M. Courty, M. Jiang, C. P. Grey, F. Dolhem, J.-M. Tarascon and P. Poizot, *J. Am. Chem. Soc.*, 2009, **131**, 8984–8988.
18 H. Chen, M. Armand, G. Demailly, F. Dolhem, P. Poizot and J. M. Tarascon, *Chemsuschem*, 2008, **1**, 348–355.
19 S. Renault, J. Geng, F. Dolhem and P. Poizot, *Chem. Commun.*, 2011, **47**, 2414–2416.
20 J. Geng, J.-P. Bonnet, S. Renault, F. Dolhem and P. Poizot, *Energy Environ. Sci.*, 2010, **3**, 1929–1933.
21 A. Abouimrane, W. Weng, H. Eltayeb, Y. Cui, J. Niklas, O. Poluektov and K. Amine, *Energy Environ. Sci.*, 2012, **5**, 9632–9638.
22 S. Wang, L. Wang, Z. Zhu, Z. Hu, Q. Zhao and J. Chen, *Angew. Chem., Int. Ed.*, 2014, **53**, 5892–5896.
23 C. Wang, Y. Xu, Y. Fang, M. Zhou, L. Liang, S. Singh, H. Zhao, A. Schober and Y. Lei, *J. Am. Chem. Soc.*, 2015, **137**, 3124–3130.
24 L. Zhao, J. Zhao, Y.-S. Hu, H. Li, Z. Zhou, M. Armand and L. Chen, *Adv. Energy Mater.*, 2012, **2**, 962–965.
25 C. Luo, Y. Zhu, Y. Xu, Y. Liu, T. Gao, J. Wang and C. Wang, *J. Power Sources*, 2014, **250**, 372–378.
26 Y. Park, D.-S. Shin, S. H. Woo, N. S. Choi, K. H. Shin, S. M. Oh, K. T. Lee and S. Y. Hong, *Adv. Mater.*, 2012, **24**, 3562–3567.
27 W. S. Hummers and R. E. Offeman, *J. Am. Chem. Soc.*, 1958, **80**, 1339.
28 S. Renault, V. A. Mihali and D. Brandell, *Electrochem. Commun.*, 2013, **34**, 174–176.
29 L. Fédèle, F. Sauvage, J. Bois, J.-M. Tarascon and M. Bécuwe, *J. Electrochem. Soc.*, 2014, **161**, A46–A52.
30 V.-A. Oltean, S. Renault, M. Valvo and D. Brandell, *Materials*, 2016, **9**, 142.
31 J. A. Kaduk, *Acta Crystallogr., Sect. B: Struct. Sci.*, 2000, **56**, 474–485.

